

## Modeling and Testing Superconducting Artificial CPW Lines Suitable for Parametric Amplification

Mena, F.P.; Valenzuela, D.; Espinoza, C.; Pizarro, F.; Tan, B.-K.; Thoen, D.J.; Baselmans, J.J.A.; Finger, R.

**DOI**

[10.1109/TASC.2024.3389652](https://doi.org/10.1109/TASC.2024.3389652)

**Publication date**

2024

**Document Version**

Final published version

**Published in**

IEEE Transactions on Applied Superconductivity

**Citation (APA)**

Mena, F. P., Valenzuela, D., Espinoza, C., Pizarro, F., Tan, B.-K., Thoen, D. J., Baselmans, J. J. A., & Finger, R. (2024). Modeling and Testing Superconducting Artificial CPW Lines Suitable for Parametric Amplification. *IEEE Transactions on Applied Superconductivity*, 34(6), Article 3500808. <https://doi.org/10.1109/TASC.2024.3389652>

**Important note**

To cite this publication, please use the final published version (if applicable).  
Please check the document version above.

**Copyright**

Other than for strictly personal use, it is not permitted to download, forward or distribute the text or part of it, without the consent of the author(s) and/or copyright holder(s), unless the work is under an open content license such as Creative Commons.

**Takedown policy**

Please contact us and provide details if you believe this document breaches copyrights.  
We will remove access to the work immediately and investigate your claim.

***Green Open Access added to TU Delft Institutional Repository***

***'You share, we take care!' - Taverne project***

**<https://www.openaccess.nl/en/you-share-we-take-care>**

Otherwise as indicated in the copyright section: the publisher is the copyright holder of this work and the author uses the Dutch legislation to make this work public.

# Modeling and Testing Superconducting Artificial CPW Lines Suitable for Parametric Amplification

F. P. Mena , D. Valenzuela , C. Espinoza , F. Pizarro , Senior Member, IEEE, B.-K. Tan , D. J. Thoen, J. J. A. Baselmans , and R. Finger

**Abstract**—Achieving amplification with high gain and quantum-limited noise is a difficult problem to solve. Parametric amplification using a superconducting transmission line with high kinetic inductance is a promising technology not only to solve this problem but also adding several benefits. Compared with other technologies, they have the potential to improve power saturation, achieve larger fractional bandwidths, and operate at higher frequencies. In this type of amplifier, the selection of the proper transmission line is a key element in its design. Given current fabrication limitations, traditional lines, such as coplanar waveguides (CPW), are not ideal for this purpose, since it is difficult to make them with the proper characteristic impedance for good matching and slow enough phase velocity for making them more compact. Capacitively loaded lines, also known as artificial lines, are a good solution to this problem. However, few design rules or models have been presented to guide their accurate design. This fact is even more crucial considering that they are usually fabricated in the form of Floquet lines that have to be designed carefully to suppress undesired harmonics appearing in the parametric process. In this article we present, first, a new modeling strategy, based on the use of electromagnetic-simulation

software, and, second, a first-principles model that facilitate and speed the design of CPW artificial lines and of Floquet lines made out of them. Then, we present comparisons with experimental results that demonstrate their accuracy. Finally, the theoretical model allows one to predict the high-frequency behavior of the artificial lines, showing that they are good candidates for implementing parametric amplifiers above 100 GHz.

**Index Terms**—Artificial transmission line, coplanar waveguides (CPW), Floquet transmission line, parametric amplification, superconductivity.

## I. INTRODUCTION

**A**MPLIFICATION of small signals and limiting the excess noise introduced by this process are ubiquitous needs of modern electronics. In some state-of-the-art applications, such as quantum computing or astronomical instrumentation, the noise introduced by the amplifier must be close to the limit imposed by quantum mechanics [1]. Achieving amplification with high gain and quantum-limited noise is a difficult problem to solve, which is even exacerbated if operation at high frequencies or large fractional bandwidths, or both, is required. Semiconductor technology, in the form of amplifiers based in high electron-mobility transistors (HEMTs), has played an important role in filling this need [1], [2]. However, the minimum noise and fractional bandwidth they can achieve are still limited, particularly at operational frequencies above  $\sim 100$  GHz [3]. One approach to solve this problem is the use of superconducting travelling-wave parametric amplifiers, which can be implemented in two ways, as an array of Josephson junctions [4] or SQUIDs [5], or as a long highly nonlinear transmission line [6].

The former implementation, on the one hand, has demonstrated quantum limited noise at low frequencies (below 10 GHz) but can handle very limited powers, making it unsuitable for some applications [4], [7]. On the other hand, amplifiers based on long superconducting transmission lines, known as traveling-wave kinetic-inductance parametric amplifiers (TKIPAs), have also demonstrated quantum-limited noise [8], [9] but have the potential advantage of being able to handle larger input powers and operating at much larger frequencies, limited only by the energy gap of the superconductor (SC) employed to fabricate them [6]. The implementation of TKIPAs requires selecting the appropriate transmission-line geometry. The first demonstration of such amplifiers used bare

Manuscript received 18 October 2023; revised 23 February 2024; accepted 28 March 2024. Date of publication 1 May 2024; date of current version 8 May 2024. This work was supported by the National Radio Astronomy Observatory, which is a facility of the National Science Foundation operated under cooperative agreement by Associated Universities, Inc. The work of F. P. Mena was partially supported in part by the ANID through Fondecyt Grant 1180700. The work of R. Finger was supported by ANID through its funds under Grant Basal FB210003, Grant Fondecyt 1221662, and Grant Fondef ID21-10359. The work of D. Valenzuela was supported by DOCTORADO BECAS CHILE 2020 under Grant 21200705. The work of F. Pizarro was supported by the ANID through Fondecyt under Grant 1221090. (Corresponding author: F. P. Mena.)

F. P. Mena and C. Espinoza are with Central Development Laboratory, National Radio Astronomy Observatory, Charlottesville, VA 22903 USA (e-mail: pmena@nrao.edu).

D. Valenzuela is with the Electrical Engineering Department, Faculty of Physical and Mathematical Sciences, University of Chile, Santiago 2007, Chile.

F. Pizarro is with the Escuela de Ingeniería Eléctrica, Pontificia Universidad Católica de Valparaíso, Valparaíso 2362804, Chile.

B.-K. Tan is with the Department of Physics (Astrophysics), University of Oxford, OX1 3RH Oxford, U.K.

D. J. Thoen is with the Instrument Science Group—Litho, Netherlands Institute for Space Research (SRON), 2333 CA Leiden, The Netherlands.

J. J. A. Baselmans is with the Instrument Science Group—Litho, Netherlands Institute for Space Research (SRON), 2333 CA Leiden, The Netherlands, and also with the Department of Electrical Engineering, Faculty of Mathematics and Computer Science (EEMCS), Delft University of Technology, 2628 CD Delft, The Netherlands.

R. Finger is with the Astronomy Department, Faculty of Physical and Mathematical Sciences, University of Chile, Santiago 1515, Chile.

Color versions of one or more figures in this article are available at <https://doi.org/10.1109/TASC.2024.3389652>.

Digital Object Identifier 10.1109/TASC.2024.3389652

CPW lines, since they are relatively easy to implement [6]. Unfortunately, given the large inductance of the SC, due to its kinetic inductance, and limitations in the geometric dimensions that can be patterned, only lines with rather large characteristic impedances (above  $150\ \Omega$ ) can be fabricated, making its matching with external circuits difficult. Furthermore, the phase velocity achieved (around  $0.1c$ , where  $c$  is the speed of light) implies that a long line is needed to obtain a reasonable gain. Capacitively loaded superconducting microstrip and CPW lines have been investigated to overcome these problems [9], [10], [11]. Artificial lines implemented using such geometries have the potential to achieve lower impedances and phase velocities below  $0.05c$  under reasonable fabrication constraints.

The easiest way to implement capacitive loads is in the form of straight stubs, similar to interdigital capacitances [9], [11], [12]. If the line is, moreover, fabricated in a CPW geometry, the result is a versatile line, which is relatively easy to fabricate. Although the design of this type of transmission lines is not trivial, few attempts have been made to provide first-principle models or methods to properly guide their design [8], [13], [14]. Filling in the need for an adequate and fast modeling tool is even more important taking into account that, to use them in parametric amplifiers, they are usually implemented in the form of periodically repeating unit cells (Floquet lines) that need to be carefully designed to achieve proper phase matching and suppress the main unwanted harmonics appearing in the parametric process [6]. Moreover, an accurate design would allow to implement lines with a precise characteristic impedance that could minimize the large gain ripples seen in traveling-wave parametric amplifiers.

In this work, we present two new design approaches and demonstrate that they can describe in an excellent fashion the transmission measurements of a set of Floquet lines made out of segments of superconducting CPW artificial lines. One approach is based in the use of electromagnetic simulation software that, at variance with other software-aided methods, does not need large computational resources, converting it in a versatile tool for aiding in design. The second approach is a first-principles model that combines a circuital model with transfer-matrix theory. In addition to being a helpful design tool, the model also demonstrates the possible use of artificial CPW lines at frequencies above 100 GHz.

## II. GEOMETRY OF THE CPW ARTIFICIAL LINE

The layout of the superconducting artificial CPW line studied in this work is presented in Fig. 1. It consists of a CPW line where straight fingers, that form capacitances with the ground, are appended perpendicularly to it. In this way, additional capacitance per unit length is added to the CPW line in order to compensate for its large kinetic inductance. In principle, thus, the length of the fingers can be used to tune the impedance and phase velocity of the line. It is for this reason that it is very important to have an accurate methodology that allows selecting their correct length for a given purpose.

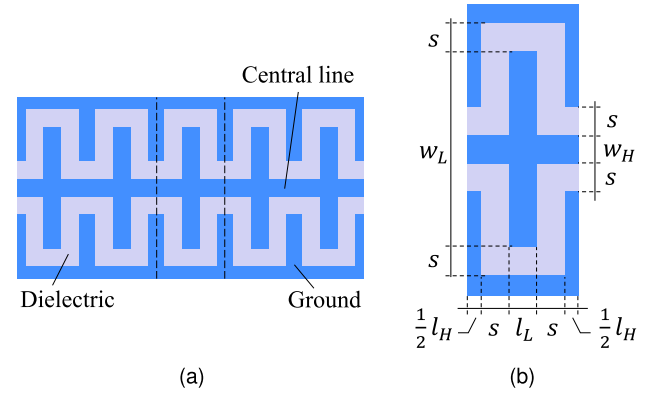


Fig. 1. (a) Capacitively-loaded artificial CPW transmission line. Vertical dashed lines indicate one unit cell. (b) Zoom of the unit cell showing the dimensions that define it.

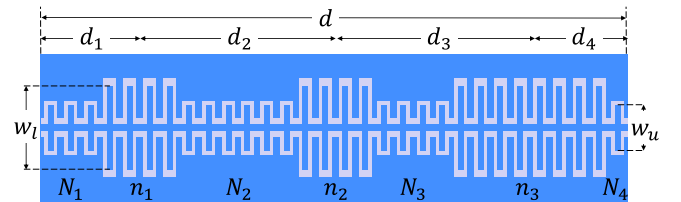


Fig. 2. Unit cell of a Floquet transmission line made out of artificial CPW lines.  $N_i$  and  $n_j$  represent the number of fingers in each segment.

## III. FLOQUET LINES WITH CPW ARTIFICIAL LINES

### A. Concept and Basic Equations

A Floquet line (for a review, see [15]) consists of unit cells that repeat periodically. In that sense, the artificial line presented in the previous section is also a Floquet line. However, to avoid confusion, here we give this name to lines made out of segments of CPW artificial lines. A scheme of the unit cell of such a Floquet line is presented in Fig. 2.

The properties of a Floquet line are completely determined by its unit cell. Indeed, let  $T_{UC}$  be the transmission matrix of the latter

$$T_{UC} = \begin{pmatrix} A & B \\ C & D \end{pmatrix}.$$

Then, if  $d$  is the length of the unit cell, the propagation constant,  $\gamma$ , and Bloch impedance,  $Z_B$ , of the entire Floquet line can be calculated from

$$\cosh \gamma d = \frac{A + D}{2} \quad (1)$$

and

$$Z_B = \pm \frac{B}{\sqrt{A^2 - 1}} \quad (2)$$

TABLE I  
PARAMETERS DEFINING THE CHARACTERIZED FLOQUET LINES

ID	$s$ μm	$w_u$ μm	$w_l$ μm	$n_1$ -	$n_2$ -	$n_3$ -	$N_1$ -	$N_2$ -	$N_3$ -	$N_4$ -	$n$ -	$d$ μm
A	1	19	35	40	40	80	110	221	201	93	62	3140
B	2	26	40	20	20	40	38	77	67	29	40	2328

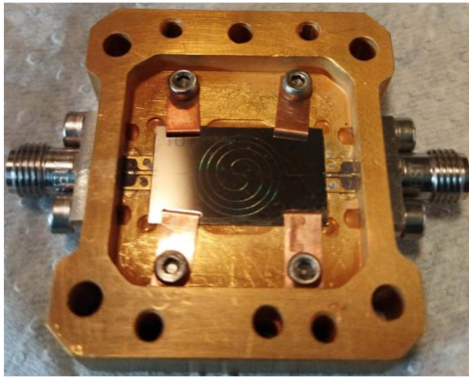


Fig. 3. Superconducting Floquet line mounted for characterization. The dimensions of the chip are 20 mm × 12 mm.

respectively. Moreover, the transmission of a Floquet line with  $n$  unit cells is given by

$$S_{21} = \frac{2Z_0 Z_B}{(Z_0^2 + Z_B^2) \sinh n\gamma d + 2Z_0 Z_B \cosh n\gamma d} \quad (3)$$

where  $Z_0$  is the impedance to which it is connected.

### B. Fabrication

Using an earlier version of the model to be presented in Section V [16], we designed and fabricated a set of the Floquet lines described above. We used Si ( $\epsilon_r = 11.44$ ) as substrate and a 60-nm superconducting layer of NbTiN deposited by the sputtering system LLS801 in static mode ( $T_c = 14.7$  K,  $\rho_n = 132 \mu\Omega\text{cm}$ ) [17]. Several versions were fabricated, all keeping  $s = l_H = l_L = w_H$ . The dimensions of the fabricated versions that are described in this article are given in Table I. A picture of one of the resulting devices mounted in a block for characterization can be seen in Fig. 3.

### C. Characterization

Some of the manufactured devices were characterized at 4 K and 100 mK in two different setups. Two examples of these measurements are presented in the gray lines of Fig. 4. To normalize the transmission, a second set of measurements was made where the mounted device was replaced by a coaxial barrel connector.

## IV. MODELING FLOQUET LINES WITH THE HELP OF ELECTROMAGNETIC SIMULATION SOFTWARE

In this section, we present two different ways of modeling the Floquet lines. Both use the results of a commercially available

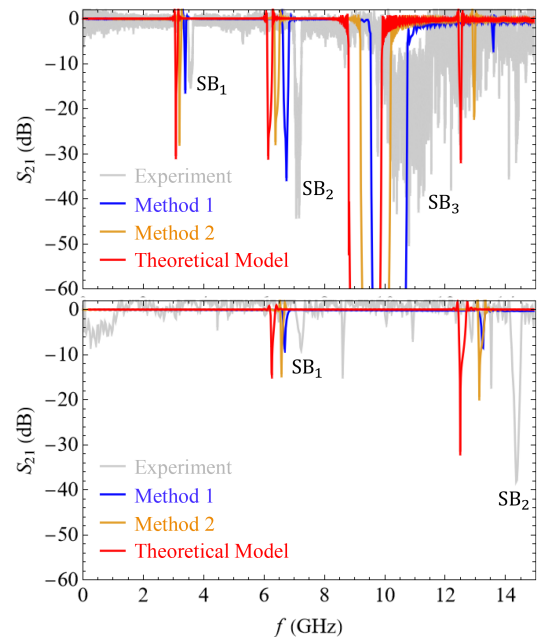


Fig. 4. Measured (gray line) and modeled transmissions of the Floquet lines presented in Table I. Stopbands in the experimental data have been marked as SB, all other features have been identified as spurious, most probably excited by the connecting bondwires. For modeling, we used software aided methods 1 (blue line) and 2 (orange line), and a first-principles model (red line). (Top) Device A characterized at 100 mK. (Bottom) Device B characterized at 4 K. The measurements were made in different experimental setups. In both panels and for all stopbands, the differences in frequency position between the experimental data and method 1, method 2, and theoretical model are 5%, 8%, and 12%, respectively. The apparent larger difference in device B is due to the higher frequency at which the stopbands appear.

electromagnetic simulation software, HFSS in this case, as an intermediate step. The CAD models used in both methods are presented in Fig. 5. The superconducting layer was modeled by assigning to it a surface impedance given by

$$Z_s = 2\pi j f \mu_0 \lambda \coth t/\lambda$$

where  $f$  is the frequency,  $\mu_0$  is the vacuum permeability,  $t$  is the thickness of the SC, and  $\lambda$  is its penetration depth [18].

### A. Method 1: Using the Simulation of a Unit Cell

Following [14], this method starts by simulating in HFSS one unit cell of the Floquet line. Then, the resulting  $S$  matrix is converted to the transmission matrix from which its propagation constant, Bloch impedance, and transmission are calculated using (1), (2), and (3), respectively. The transmissions of devices A and B obtained after applying this method are presented in the blue lines of Fig. 4. The agreement between the method and

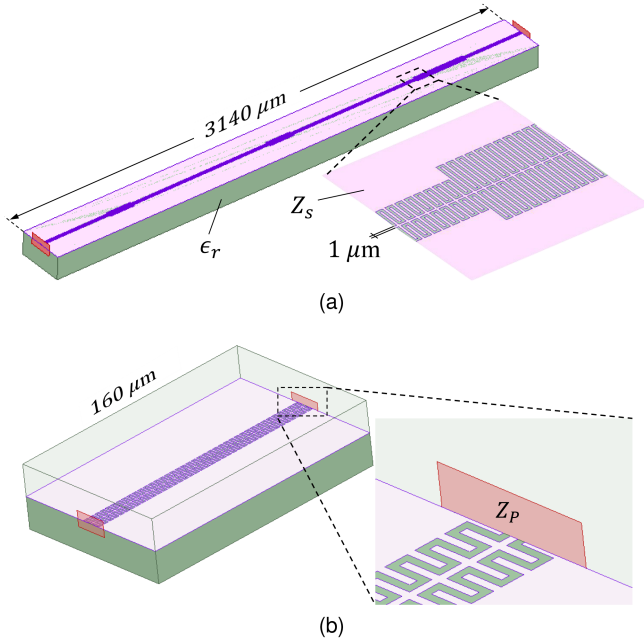


Fig. 5. Examples of CAD models used in the simulations with HFSS. The dielectric has a permittivity  $\epsilon_r$ , and the SC a surface impedance  $Z_S$ . The insets show the smallest features of the models. (a) The unit cell of device A. (b) One of the simulated homogeneous artificial CPW lines. The excitation port of the model has an impedance  $Z_P$  that, in general, is different from the impedance of the line,  $Z_0$ . The latter is obtained through the process described in Section IV-B.

the measurements is excellent, validating the former. In fact, the difference between the measured and predicted position of the stopbands in all cases is of only  $\Delta f_{SB} = 5\%$ . Further simulations, not presented here, demonstrate that decreasing the convergence criterion 10 times improves the agreement to  $\Delta f_{SB} = 3\%$ .

Unfortunately, there is one major disadvantage of using this method. Given the large dimensions of the unit cell with respect to its smallest features, it requires a large amount of computational resources, which, in turn, makes it impractical for design. For example, simulation of the unit cell of device A [Fig. 5(a)], with a convergence criterion of  $\Delta S = 0.1$ , needed to obtain the results presented in the top panel of Fig. 4, took approximately 30 min per frequency point using a desktop computer with a processor Intel Xeon W-2295 running at 3.00 GHz and a RAM of 128 GB.

### B. Method 2: Using the Simulation of Homogeneous Artificial CPW Lines

If the transmission matrix,

$$T_i = \begin{pmatrix} \cosh \gamma_i l_i & Z_{0,i} \sinh \gamma_i l_i \\ \frac{1}{Z_{0,i}} \sinh \gamma_i l_i & \cosh \gamma_i l_i \end{pmatrix} \quad (4)$$

of every segment forming the unit cell of a Floquet line is known, they can be multiplied to obtain the transmission matrix of the unit cell. With this matrix, the properties of the Floquet line are completely determined.

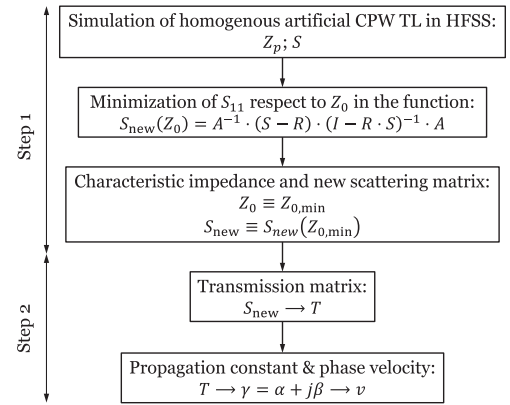


Fig. 6. Flowchart summarizing the procedure to obtain the characteristic impedance and phase velocity of a homogeneous artificial CPW transmission line. All quantities are defined in the text.

Having demonstrated in the previous section the good accuracy of HFSS in describing Floquet superconducting lines, we have used it to determine the propagation constants and characteristic impedances needed to construct the matrices (4). The method, summarized in Fig. 6, consists of two steps.

First, we need to realize that HFSS, or any other electromagnetic software used in the way described here, cannot directly give the impedance of any artificial line,  $Z_0$ , as the one depicted in Fig. 5(b). In fact, the impedance of the port,  $Z_P$ , calculated by HFSS corresponds to that of the small CPW section connected directly to it. If  $S$  is the scattering matrix given by HFSS, we assert that  $Z_0$  corresponds to the impedance that minimizes  $S_{new,11}$  in the renormalization expression

$$S_{new} = A^{-1} \cdot (S - R) \cdot (I - R \cdot S)^{-1} \cdot A$$

where  $I$  is the unit matrix,  $A = \frac{\sqrt{Z_0 - Z_P}}{Z_0 + Z_P} I$ , and  $R = \frac{Z_0 - Z_P}{Z_0 + Z_P} I$ .

Second, after converting  $S_{new}$  to a transmission matrix, it is possible to obtain the propagation constant according to (4). An example of the use of this two-step process is presented in Fig. 7. Importantly, although the minimization was with respect to the parameter  $S_{11}$ , it has to be noted that it also maximizes  $S_{21}$ .

For designing an artificial CPW line, one must realize that if the internal dimensions are kept constant, its properties can be tuned by varying  $w_L$ . Given the much less demanding computational resources needed for the required simulations, this method can be applied to obtain the necessary information, as presented in the empty symbols of Fig. 8. Remarkably, when  $w_L \rightarrow w_H$ , the values obtained by method 2 tend to those calculated for a CPW line with the dimensions of the central line. Fig. 8 also shows that it is indeed possible to obtain 50- $\Omega$  lines with this geometry together with a low phase velocity.

Using the values obtained in Fig. 8, the transmissions of the constructed devices were calculated and are presented in the orange lines of Fig. 4. The agreements with experiment and model 1 are also good, with a difference in the position of the stopbands of 8% and 6%, respectively. The deviations between models 1 and 2 may be due to the fact that the electromagnetic simulation of the entire unit cell can capture small interactions

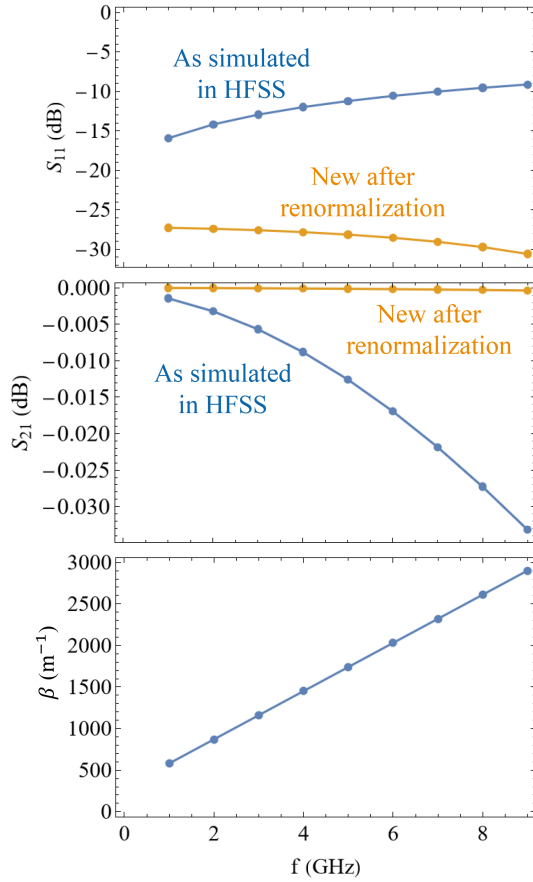


Fig. 7. Example of applying HFSS software-aided method 2 to an artificial CPW line with  $s = l_H = l_L = w_H = 1 \mu\text{m}$  and  $w_L = 19 \mu\text{m}$ , i.e., the central line of device A. (Top) Reflection before (blue line) and after (orange line) applying renormalization. (Middle) Transmission before (blue line) and after (orange line) applying renormalization. (Bottom) Imaginary part of the propagation constant. The slope of the line correspond to a phase velocity of  $v = 0.07 c$ .

between the loads and the central line, which are not taken into account during multiplication of the transmission matrices. Supporting this idea, we have observed that simulations of new designs with narrower loads (i.e., smaller  $w_L$ ) show a better agreement between models 1 and 2. The difference in stopband position can be as low as 2%.

## V. FIRST-PRINCIPLES MODEL OF A CPW ARTIFICIAL LINE

### A. Description of the Model

The model presented here shares some similarities with work presented before [8], [13], [16]. However, as discussed in the following, we describe most of the elements of the model as transmission lines and not as lumped elements. In fact, when comparing different versions, we found that the former described the simulations and experimental results with more accuracy.

Let us consider a unit cell of the CPW artificial line. As depicted in Fig. 9, the unit cell can be divided into several elements, discussed below, to form a circuitual model. Then, we can use standard microwave transfer-matrix theory to obtain the transmission matrix of the unit cell which, in turn, allows us to

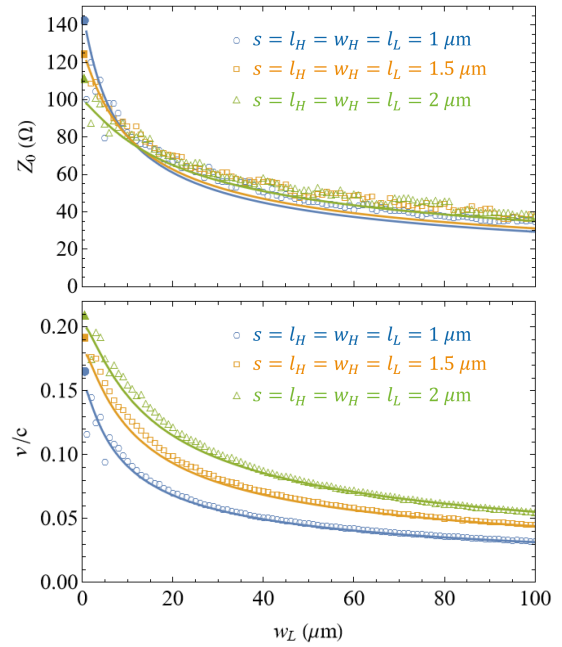


Fig. 8. Dependence of the properties of a homogenous artificial CPW line with  $w_L$  (see Fig. 1). This dependence was obtained using software-aided method 2 (empty symbols) and the first-principles model (lines). Solid symbols on the far left are the theoretical values of a CPW line, calculated according to [19], that has the dimensions of the central line, i.e., when  $w_L \rightarrow 0$ . (Top) Characteristic impedance. (Bottom) Phase velocity as fraction of the speed of light.

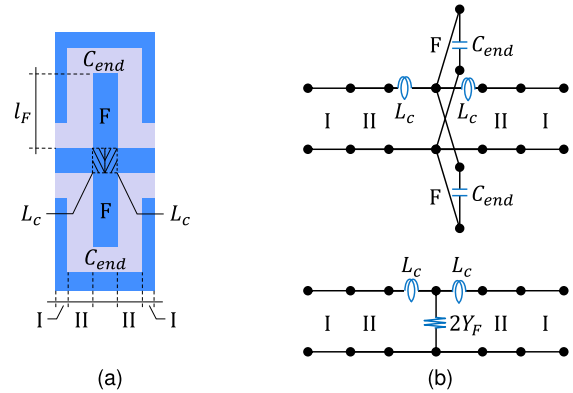


Fig. 9. (a) Unit cell of the artificial CPW transmission line identifying the elements that are included in the equivalent circuit model: CPW lines I, II, and F, capacitance at the end of the capacitive load,  $C_{\text{end}}$ , and a free-standing SC of inductance  $L_c$ . Line F has a length  $l_F = \frac{1}{2}(w_L - w_H)$ . (b) Top panel presents the corresponding circuit model, which can be reduced to the one presented in the bottom panel.

use expressions (1), (2), and (3) to determine the properties of the entire line.

Elements I and II are short CPW lines of lengths  $\frac{1}{2}l_H$  and  $s$ , respectively. Their propagation constant and characteristic impedance, needed to form their transmission matrices, can be calculated using theoretical models for superconducting CPW lines [19].

Elements F are CPW stubs of length  $l_F$  terminated in a capacitance  $C_{\text{end}}$ . Since they are in parallel, they can be replaced

by an admittance equal to two times the admittance

$$Y_F = Y_{0F} \frac{Y_{\text{end}} + Y_{0F} \tanh \gamma_F l_F}{Y_{0F} + Y_{\text{end}} \tanh \gamma_F l_F}$$

where  $Y_{0F} = 1/Z_{0F}$  is the characteristic admittance of the stub,  $\gamma_F$  is its propagation constant, and  $Y_{\text{end}} = j2\pi f C_{\text{end}}$ . The capacitance  $C_{\text{end}}$  can be calculated from expressions obtained using conformal techniques [12].

While studying this model, we realized that, for good accuracy, it was not possible to neglect the effect of the intersection between the central line and the capacitive loads. Although the strong effect of this intersection can be the result of electromagnetic interaction between the load and the central line, we found that two simplified models can be used with good results. One of the models simply considers that the transmission line II of Fig. 9 has a length  $s + l_L/2$  instead of only  $s$ . The second option, discussed in the rest of this article, is to divide the intersection into two free-standing SC thin sheets. There are three contributions to the impedance per unit length of a free standing SC of width  $w$  [20]

$$\begin{aligned} \frac{L_c}{l} = & \frac{\mu_0}{8\pi} + \frac{\mu_0}{2\pi} \left( \log \frac{2l}{t+w} + 0.2235 \frac{t+w}{l} + \frac{1}{2} \right) \\ & + \frac{\mu_0 \lambda^2}{wt}. \end{aligned} \quad (5)$$

The first term represents the magnetic field inside the sheet. The second one is its self inductance [21]. The last term is the kinetic inductance per unit length of the superconducting sheet when there is a uniform current distribution through it.

### B. Comparison With HFSS Simulations

Here, we present comparisons between the theoretical model described above and the software-aided modelling method 2 presented in Section IV-B. First, using the theoretical model we studied the dependence of  $Z_0$  and  $v/c$  on the length  $w_L$  for the same lines studied in Fig. 8. For easier comparison, the results are presented in the same figure as solid lines. Both modeling methods show excellent agreement, especially for values  $w_L > 30 \mu\text{m}$ .

For the second comparison, we need first to realize that the first-principles model can be applied without major changes to artificial CPW lines made of a perfect electrical conductor (PEC) instead of a SC. Therefore, it can be applied at the same time, without changing any parameter, to both types of lines if they have the same geometrical dimensions. Then, we also applied software-aided modeling method 2 to lines made of PEC. The results and comparison between lines made out of PEC and superconducting material are presented in Fig. 10. Once again, the agreement is excellent, demonstrating the consistency of the theoretical model.

### C. Comparison With Measurements

Using the theoretical model, we also calculated the transmission of the Floquet lines that were characterized and presented in Section III-C. The results, presented as red solid lines in Fig. 4, show a reasonable agreement with the measurements

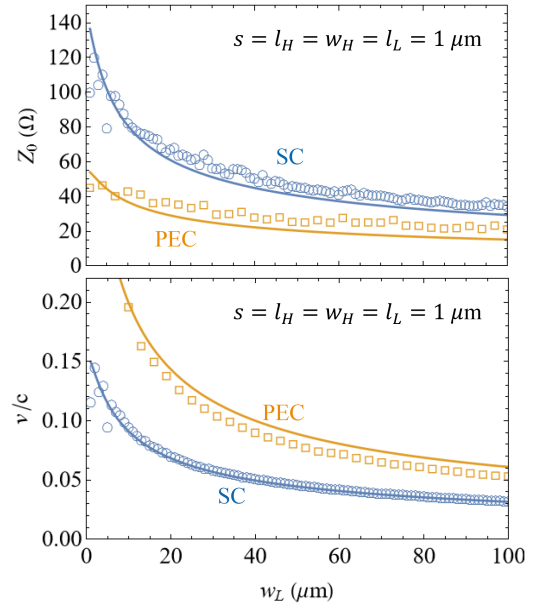


Fig. 10. Comparison between software-aided model method 2 (empty symbols) and first-principles model (lines). Both models were applied to lines using a SC and a PEC. (Top) Characteristic impedance. (Bottom) Phase velocity as fraction of the speed of light.

( $\Delta f_{\text{SB}} = 12\%$ ). The agreement of the theoretical model with experiment can be improved in an ad-hoc manner by adding a weight to the contribution given by (5). However, this contraption only reflects the difficulty of modeling the intersection of the capacitive fingers with the central line.

## VI. PREDICTED PERFORMANCE AT HIGH FREQUENCIES

Assuming a single mode propagation, the theoretical model presented in previous section can predict the performance of superconducting artificial CPW lines at high frequencies. The results are presented in Fig. 11 (solid lines). We can see that if no other mode is excited, the propagating mode shows a small dispersion of up to a few hundred GHz. These results are corroborated by applying method 2 (Section IV-B), in windows of 20 GHz, in order to obtain the wavenumber and characteristic impedance of an the artificial line with  $s = 1 \mu\text{m}$  [see Fig. 5(b)]. The calculated values, presented as circles in Fig. 11, agree fairly well with the theoretical model.

For the purpose of determining the influence of other modes, we applied the multimodal transfer matrix (MTM) method [22], [23] to the same artificial line. Two modes, identified as symmetric and asymmetric CPW, were used in the calculations. The resulting wavenumber is presented as the solid line of Fig. 12. Up to the highest simulated frequency, the influence of the antisymmetrical mode was found to be minimal. Moreover, the results coincide very well with the simulation method 2 (open circles), confirming that the transmission is monomodal with small dispersion up to few hundred GHz. These features make the artificial CPW line a good candidate to implement superconducting parametric amplifiers at high frequencies.



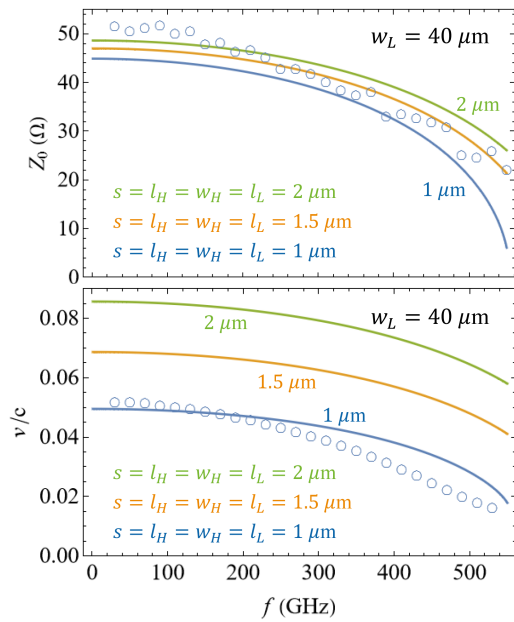


Fig. 11. Behaviour of superconducting CPW artificial lines at high frequencies extracted from the first-principles model (lines) and from applying method 2 in windows of 20 GHz (circles). The latter was applied only to an artificial line with  $s = 1 \mu\text{m}$ . (Top) Characteristic impedance. (Bottom) Phase velocity as fraction of the speed of light.

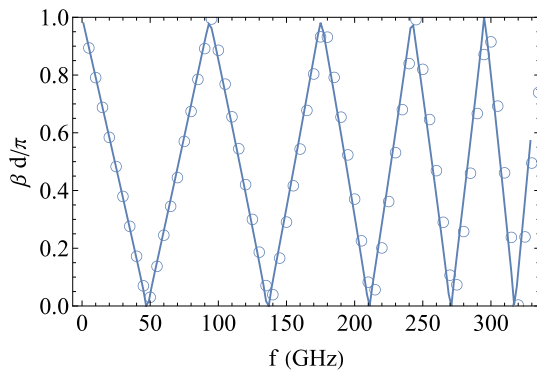


Fig. 12. Wavenumber of the artificial line with  $s = l_H = l_L = w_H = 1 \mu\text{m}$  and  $w_L = 40 \mu\text{m}$ . The calculations were made using the MTM method (line) and method 2 described in this work (circles). The latter data correspond to those presented in Fig. 11.

## VII. CONCLUSION

We have presented two strategies for designing superconducting artificial lines and Floquet lines made out of them. The first strategy combines the use of electromagnetic simulation software with standard transfer-matrix theory. The former is used to extract the properties of the artificial line that, in turn, allow the use of the latter to describe Floquet lines. In contrast with other methods, it requires much less computational resources since it does not require the simulation of the entire unit cell of a Floquet line. The second strategy uses first principles to construct an equivalent circuit model. Furthermore, these strategies were compared against each other, showing excellent agreement. We have also demonstrated that both of them describe very well the measured transmission of superconducting Floquet lines

fabricated using NbTiN. One of the main advantages of using the design strategies presented in this work is that they allow a fast modeling of Floquet lines made out of CPW artificial lines, which is important in, for example, the design of travelling-wave parametric amplifiers. Finally, using the first-principles model we showed that the CPW artificial line is a good candidate to implement parametric amplifiers at frequencies of few hundred GHz.

## ACKNOWLEDGMENT

The authors would like to thank SRON and the Kavli Institute of Nanoscience Delft for the use of their clean room facilities for device fabrication. The author F. P. Mena would like to thank C. Jarufe for his fruitful discussions.

## REFERENCES

- [1] J. C. Bardin, "Cryogenic low-noise amplifiers: Noise performance and power dissipation," *IEEE Solid-State Circuits Mag.*, vol. 13, no. 2, pp. 22–35, 2021.
- [2] M. W. Pospieszalski, "Extremely low-noise cryogenic amplifiers for radio astronomy: Past, present, and future," in *Proc. 22nd Int. Microw. Radar Conf.*, 2018, pp. 1–6.
- [3] M. W. Pospieszalski, "On the limits of noise performance of field effect transistors," in *Proc. IEEE MTT-S Int. Microw. Symp.*, 2017, pp. 1953–1956.
- [4] J. Aumentado, "Superconducting parametric amplifiers: The state of the art in Josephson parametric amplifiers," *IEEE Microw. Mag.*, vol. 21, no. 8, pp. 45–59, Aug. 2020.
- [5] A. B. Zorin, "Josephson traveling-wave parametric amplifier with three-wave mixing," *Phys. Rev. Appl.*, vol. 6, Sep. 2016, Art. no. 034006, doi: [10.1103/PhysRevApplied.6.034006](https://doi.org/10.1103/PhysRevApplied.6.034006).
- [6] B. H. Eom et al., "A wideband, low-noise superconducting amplifier with high dynamic range," *Nature Phys.*, vol. 8, pp. 623–627, 2012.
- [7] M. Esposito, A. Ranadive, L. Planat, and N. Roch, "Perspective on traveling wave microwave parametric amplifiers," *Appl. Phys. Lett.*, vol. 119, no. 12, 2021, Art. no. 120501, doi: [10.1063/5.0064892](https://doi.org/10.1063/5.0064892).
- [8] M. Malnou et al., "Three-wave mixing kinetic inductance traveling-wave amplifier with near-quantum-limited noise performance," *PRX Quantum*, vol. 2, Jan. 2021, Art. no. 010302, doi: [10.1103/PRXQuantum.2.010302](https://doi.org/10.1103/PRXQuantum.2.010302).
- [9] N. Klimovich, P. Day, S. Shu, B. H. Eom, H. Leduc, and A. Beyer, "Demonstration of a quantum noise limited traveling-wave parametric amplifier," 2023, *arXiv:2306.11028*.
- [10] A. A. Adamyan, S. E. de Graaf, S. E. Kubatkin, and A. V. Danilov, "Superconducting microwave parametric amplifier based on a quasi-fractal slow propagation line," *J. Appl. Phys.*, vol. 119, no. 8, 2016, Art. no. 083901, doi: [10.1063/1.4942362](https://doi.org/10.1063/1.4942362).
- [11] S. Chaudhuri et al., "Broadband parametric amplifiers based on nonlinear kinetic inductance artificial transmission lines," *Appl. Phys. Lett.*, vol. 110, no. 15, 2017, Art. no. 152601, doi: [10.1063/1.4980102](https://doi.org/10.1063/1.4980102).
- [12] H. Yoon, K. J. Vinoy, and V. K. Varadan, "Design and development of micromachined bilateral interdigital coplanar waveguide RF phase shifter compatible with lateral double diffused metal oxide semiconductor voltage controller on silicon," *Smart Mater. Structures*, vol. 12, no. 5, Sep. 2003, Art. no. 769, doi: [10.1088/0964-1726/12/5/014](https://doi.org/10.1088/0964-1726/12/5/014).
- [13] K. Nakagawa, M. Takeda, A. Saito, and H. Terai, "Transmission properties of fishbone-type superconducting transmission lines," *Japanese J. Appl. Phys.*, vol. 59, no. 11, Oct. 2020, Art. no. 110904, doi: [10.35848/1347-4065/abbf65](https://doi.org/10.35848/1347-4065/abbf65).
- [14] B. Tan, F. Boussaha, C. Chaumont, J. Longden, and J. N. Montilla, "Engineering the thin film characteristics for optimal performance of superconducting kinetic inductance amplifiers using a rigorous modelling technique," *Open Res. Europe*, vol. 2, 2022, Art. no. 88.
- [15] J. Perruisseau-Carrier, "Periodic structure transmission line theory," in *Microwave Periodic Structures Based on MicroElectroMechanical Systems (MEMS) and Micromachining Techniques*. Lausanne, Switzerland: EPFL, 2007, ch. 1, pp. 25–64. [Online]. Available: <http://infoscience.epfl.ch/record/112718>

- [16] F. Mena and D. Valenzuela, "Modelling of travelling-wave kinetic inductance parametric amplifiers implemented with artificial transmission lines," in *Proc. 31st Int. Symp. Space Terahertz Technol.*, 2020, Art. no. 93. [Online]. Available: <https://www.nrao.edu/meetings/isstt/proceed/2020Proceedings.pdf>
- [17] D. J. Thoen, B. G. C. Bos, E. A. F. Haalebos, T. M. Klapwijk, J. J. A. Baselmans, and A. Endo, "Superconducting NbTiN thin films with highly uniform properties over a  $\emptyset$  100 mm wafer," *IEEE Trans. Appl. Supercond.*, vol. 27, no. 4, Jun. 2017, Art. no. 1500505.
- [18] A. Kerr, "Surface impedance of superconductors and normal conductors in EM simulators," National Radio Astronomy Observatory, Charlottesville, VA, USA, Tech. Rep. 245, Jan. 1999. [Online]. Available: <http://www.mma.nrao.edu/memos/html-memos/ma245/memo245.pdf>
- [19] K. Watanabe, K. Yoshida, and T. A. Kohjiro, "Kinetic inductance of superconducting coplanar waveguides," *Japanese J. Appl. Phys.*, vol. 33, no. 10R, Oct. 1994, Art. no. 5708, doi: [10.1143/JJAP.33.5708](https://doi.org/10.1143/JJAP.33.5708).
- [20] S. K. Tolpygo, E. B. Golden, T. J. Weir, and V. Bolkhovsky, "Mutual and self-inductance in planarized multilayered superconductor integrated circuits: Microstrips, striplines, bends, meanders, ground plane perforations," *IEEE Trans. Appl. Supercond.*, vol. 32, no. 5, Aug. 2022, Art. no. 1400331.
- [21] E. Rosa, "The self and mutual inductances of linear conductors," *Bull. Bur. Standards*, vol. 4, no. 2, pp. 301–344, 1908. [Online]. Available: [https://nvlpubs.nist.gov/nistpubs/bulletin/04/nbsbulletinv4n2p301\\_a2b.pdf](https://nvlpubs.nist.gov/nistpubs/bulletin/04/nbsbulletinv4n2p301_a2b.pdf)
- [22] F. Mesa, G. Valerio, R. Rodríguez-Berral, and O. Quevedo-Teruel, "Simulation-assisted efficient computation of the dispersion diagram of periodic structures: A comprehensive overview with applications to filters, leaky-wave antennas and metasurfaces," *IEEE Antennas Propag. Mag.*, vol. 63, no. 5, pp. 33–45, Oct. 2021.
- [23] F. Giusti, Q. Chen, F. Mesa, M. Albani, and O. Quevedo-Teruel, "Efficient Bloch analysis of general periodic structures with a linearized multimodal transfer-matrix approach," *IEEE Trans. Antennas Propag.*, vol. 70, no. 7, pp. 5555–5562, Jul. 2022.

**F. P. Mena** received the B.S. degree in physics from Escuela Politécnica Nacional, Quito, Ecuador, in 1994, and the M.S. and Ph.D. degrees in physics from the University of Groningen, Groningen, The Netherlands, in 2000, and 2004, respectively.

In 2004, he joined the Netherlands Institute for Space Research (SRON), Groningen, The Netherlands, as an Instrument Scientist with the Low Energy Division. From 2008 to 2020, he was with Universidad de Chile, where he cofounded the Radio Astronomical Instrumentation Group and the Millimeter/Submillimeter Wave Laboratory. He is currently a Scientist/Research Engineer with the National Radio Astronomy Observatory, Charlottesville, VA, USA. His research interests include the design, fabrication, and characterization of components and systems used in radio astronomical instrumentation.

**D. Valenzuela** is currently working toward the Ph.D. degree in the study and development of traveling-wave kinetic inductance parametric amplifiers with the Universidad de Chile, Santiago, Chile.

His dissertation consists of the design and characterization of parametric amplifiers using artificial CPW lines and comparison with other transmission lines. He has worked with the Millimeter Wave Laboratory, Universidad de Chile, in superconducting materials, microwave measurements, high-frequency circuits, and microwave simulation software. He has also worked with the Space and Planetary Exploration Laboratory, Universidad de Chile, in the camera software for SUCHAI I and the communication system for SUCHAI II.

**C. Espinoza** received the M.Sc. degree in electrical engineering from the Universidad de Chile, Santiago, Chile, in 2021.

Since 2017, he has been working on the development of microwave components with the Millimeter Wave Laboratory, University of Chile. Among the microwave projects in which he has been involved are the development of ALMA Band 2+3 amplifiers and mixers, digitally aided mixers, and 5G antennas. In 2023, he joined NRAO to focus his work on cryogenic-operated parametric amplifiers.

**F. Pizarro** (Senior Member, IEEE) received the B.Sc. degree in electronic engineering from the Pontificia Universidad Católica de Valparaíso, Valparaíso, Chile, in 2010, the M.Sc. degree in telecommunications engineering from the Politecnico di Torino, Turin, Italy, in 2010, and the Ph.D. degree in electromagnetism and high-frequency systems, plasma engineering from the Institut Supérieur de l'Aéronautique et de l'Espace, Toulouse, France, in 2014.

Since 2014, he has been an Associate Professor with the School of Electrical Engineering, Pontificia Universidad Católica de Valparaíso. His research interests include 3D-printed antennas, metamaterials, and plasma/microwave interaction.

**B.-K. Tan** received the D.Phil. degree in astrophysics from the University of Oxford, Oxford, U.K., in 2012.

He is currently with the Department of Physics (Astrophysics), University of Oxford. His main research interests include the development of ultra-sensitive superconducting quantum electronic devices, such as millimetre and submillimetre detectors, terahertz components and broadband superconducting quantum amplifiers, for astronomy, quantum information technologies, and fundamental physics experiments.

**D. J. Thoen** received the B.Sc. degree in applied physics from Fontys University, Eindhoven, The Netherlands, in 2008.

He is a Senior Process Engineer. Since 2023, he has been leading the Nano Development Section with SRON Netherlands Institute of Space Research, Leiden, The Netherlands. He is a Guest-Employee with the Delft University of Technology, Delft, The Netherlands, and Leiden University, Leiden and is Founder/CEO of Thoen Tech Consultancy.

**J. J. A. Baselmans** received the graduation and Ph.D. (summa cum laude) degrees in physics from the University of Groningen in 1998 and 2002, respectively.

He is Senior Instrument Scientist with the SRON Netherlands Institute for Space Research, Leiden, The Netherlands, and Full Professor in experimental astronomy with the THz sensing group at the Delft University of Technology, Delft, The Netherlands. He started in 2002 as Postdoctoral Instrument Scientist with SRON Netherlands Institute for Space Research, where he has worked until 2004 on Hot Electron Bolometer mixers. Since then, he leads the Dutch effort on Kinetic Inductance Detectors. He pioneered the concept of the on-chip spectrometer for far-infrared radiation detection and is a Lead System Engineer for the first on-chips spectrometer instrument, Deshima. He is also the Detector Lead for the AMKID camera on APEX and has pushed MKID technology to sensitivity levels suitable for future cryogenically cooled space-based observatories. During his Ph.D., he studied the superconducting state in normal metal Josephson junctions. He has authored or coauthored more than 100 papers.

**R. Finger** received the Ph.D. degree in electrical engineering and a double major in engineering and physics from Universidad de Chile, Santiago, Chile, in 2013.

He is an Associate Professor with the Department of Astronomy, Universidad de Chile. He develops antennas, receivers, and digital signal processors for Radio Astronomy and other applications. He has worked in USA, Sweden, U.K., and at the ALMA Observatory in Chile. He leads the Millimeter Wave Laboratory of the Center for Astrophysics and Associated Technologies, where he develops technology from centimeter to sub-millimeter wavelengths.